New ²⁶Al/¹⁰Be and (U-Th)/He constraints on the age of the Upland Complex, central Mississippi River Valley William Odom ^a, Florian Hofmann ^b, Roy Van Arsdale ^c, Darryl Granger ^a ^a Department of Earth, Atmospheric, and Planetary Sciences, Purdue University, West Lafayette, IN 47907, USA ^b Division of Geological and Planetary Sciences, California Institute of Technology, 1200 E California Blvd, Pasadena, CA 93225, USA; now at: Department of Earth and Environmental Sciences, University of Munich, Luisenstr. 37, 80333 Munich, Germany ^c Department of Earth Sciences, University of Memphis, Memphis, TN 38152, USA Corresponding author: William Odom (odomw@purdue.edu)

Abstract

25	The Upland Complex is a widespread terrace of the ancestral Mississippi River. It has
26	played a central role in studies of the Pliocene Mississippi River drainage, as well as uplift and
27	seismicity in the central Mississippi River Valley. Previous efforts to date the Upland Complex
28	have yielded a range of age estimates spanning the Miocene through Pleistocene. We dated
29	gravels and Fe-oxide cements from quarries of the Upland Complex in Arkansas, Kentucky,
30	Mississippi, and Tennessee using ²⁶ Al/ ¹⁰ Be burial dating and (U-Th)/He geochronology. Our
31	²⁶ Al/ ¹⁰ Be burial dates revealed possible Pliocene-to-Pleistocene depositional ages, while (U-
32	Th)/He dating showed that the onset of weathering dates to at least the Pliocene. Taken together,
33	the ²⁶ Al/ ¹⁰ Be and (U-Th)/He age constraints demonstrate that the Upland Complex is at least
34	Pliocene in age, and likely formed during a prolonged period of base level stability that preceded
35	Pleistocene glaciations.
36	
37	Keywords: Upland Complex, cosmogenic, burial dating, (U-Th)/He, geochronology, Pliocene
38	
39	Highlights
40	• ²⁶ Al/ ¹⁰ Be and (U-Th)/He dates provide a Pliocene minimum age for the Upland Complex
41	• The Upland Complex is likely mid-Pliocene and is no older than Late Miocene
42	• Formation of the Upland Complex may be related to widespread Pliocene aggradation
43	
44	
45	
46	

1. Introduction

47

48

49

50

51

52

53

54

55

56

57

58

59

60

61

62

63

64

65

66

67

68

69

The Upland Complex of the central Mississippi River Valley is a high-level terrace of the ancestral Mississippi River (Autin et al., 1991; Van Arsdale et al., 2007; Lumsden et al., 2016). This dominantly sand and gravel terrace deposit has been mapped from Illinois to Louisiana and has been assigned different names in different states. In Illinois and Missouri it is the Mounds gravel (Willman and Frye, 1970; Harrison, et al., 1999), in Kentucky the Lafayette gravel (Potter, 1955a; 1955b) and subsequently the Continental deposits (Olive, 1980), in Arkansas and Tennessee the Upland Complex (Autin et al., 1991; Saucier, 1994), and in Mississippi the preloess sand and gravel (Dockery, 1996). The Upland Complex is particularly important for several reasons beyond its significant economic value as the primary source of gravel over its extent (Van Arsdale et al., 2012; Behrman et al., 2019). It has been interpreted to be the southern remnant of a much larger Pliocene Mississippi River floodplain and drainage basin that extended well into Canada (Cox et al., 2014; Cupples and Van Arsdale, 2014; Lumsden et al., 2016). Van Arsdale and Cupples (2013) used the base of the Upland Complex as a structural datum to identify Quaternary fault displacement within the central Mississippi River Valley. Additionally, the base of the Upland Complex's elevation 70 m above the Holocene Mississippi River near Memphis, Tennessee, has been attributed to Quaternary isostatic uplift initiated by Pleistocene sea level decline and commensurate ancestral Ohio and Mississippi river incision. This regional erosion and isostatic uplift may be contributing to Quaternary faulting and ongoing seismicity in the New Madrid seismic zone (Calais et al., 2010; Van Arsdale et al., 2019). Furthermore, Pleistocene erosion of the Upland Complex would have contributed a significant volume of sediment (>11,460 km³) to the Pleistocene Mississippi River delta (Van Arsdale et al., 2019).

The Upland Complex is interpreted to be the remnant of a floodplain that once formed a continuous ~150 m thick blanket (Van Arsdale et al., 2019), extending at least 100 km east-west from western Tennessee to Crowley's Ridge in eastern Arkansas, and 700 km north-south along the Mississippi River (Saucier and Snead, 1989; Autin et al., 1991; Van Arsdale et al., 2007; Cox et al., 2014; Cupples and Van Arsdale, 2014; Lumsden et al., 2016). It consists of fluvial gravel and fine-to-coarse-grained quartz sand with minor silt and clay (Autin et al., 1991). Grain diameters are generally less than 2 cm, but individual clasts up to 60 cm in diameter are present (Russell, 1987). Typically, >80% of the gravel consists of well-rounded chert coated with Fe oxides, with the remainder consisting of well-rounded quartz and quartzite (Potter, 1955a; Guccione et al., 1990). The polished red-brown patina on the chert shows no percussion marks, indicating that it is post-depositional (Lumsden et al., 2016). The Upland Complex is capped by a ~2 m thick. Fe-rich paleosol disconformably buried beneath Pleistocene loess that dates up to 250 ka (Markewich et al., 1992). At the base of the Upland Complex is a southsloping, relatively flat disconformity that overlies Paleogene formations (Saucier, 1994; Van Arsdale et al., 2007). Given the widespread nature of this deposit, its apparent deposition near the Pliocene-Pleistocene climatic transition, and its proposed triggering relationship with the New Madrid seismic zone (Van Arsdale et al., 2019), constraining the age of the Upland Complex has significant implications for the geomorphic and geodynamic history of central North America. Proposed depositional ages range from Miocene (May, 1981) to Pliocene (Potter, 1955b; Anthony and Granger, 2006; Van Arsdale et al., 2007; 2019), early Pleistocene (Fisk, 1944; Doering, 1958), and Pliocene-Pleistocene (Autin et al., 1991; Rovey and Spoering, 2020). In this paper we present new age determinations for several quarries in Arkansas, Kentucky,

70

71

72

73

74

75

76

77

78

79

80

81

82

83

84

85

86

87

88

89

90

91

Mississippi, and Tennessee. We use ²⁶Al/¹⁰Be burial dating to constrain minimum and maximum depositional times (supplementing previous work of Van Arsdale et al., 2014) and (U-Th)/He geochronology to provide a minimum age for the terrace from the crystallization of pedogenic goethite cement.

2. Methods

2.1.1. Cosmogenic ²⁶Al/¹⁰Be burial dating

We directly dated terrace deposits of the Upland Complex using the cosmogenic nuclides 26 Al and 10 Be. Cosmogenic nuclides are rare isotopes that are produced by the interaction of high-energy cosmic particles with Earth's atmosphere and rocks. Most surficial production of in-situ cosmogenic 26 Al and 10 Be is driven by spallation caused by cosmic-ray produced neutrons. In quartz, spallation of silicon forms 26 Al ($t_{1/2}$ = 0.705 My), while spallation of oxygen forms 10 Be ($t_{1/2}$ = 1.389 My) (Nishiizumi, 2004; Chmeleff et al., 2010; Korschinek et al., 2010). Below ~3 m of rock, production of cosmogenic nuclides via neutron spallation falls below approximately 1% its surficial value and most production occurs via muon interactions. Muons are secondary cosmic rays produced in the upper atmosphere, and cosmogenic nuclides may be produced from high energy muon reactions or capture of low energy muons. Because muons can penetrate significantly deeper than neutrons – on the order of hundreds of meters – they are an important consideration for post-burial production of cosmogenic nuclides in buried deposits.

2.1.2. Minimum burial age dating

The simplest form of burial dating works under the assumption that buried sediments originated from a steadily eroding landscape. In this scenario, the concentrations of ²⁶Al and

116 ¹⁰Be are functions of the cosmogenic nuclide production rates and rock erosion rates. The
 117 preburial concentration of a given nuclide is modeled by the equation:

$$N_{i,inh} = \frac{P_i}{\frac{1}{\tau_i} + \frac{\rho E}{\Lambda}}$$
 (1)

where $N_{i,inh}$ is the inherited (pre-burial) concentration of the nuclide (at/g), P_i is the production rate of the nuclide (at/g/yr), τ_i is the radioactive mean-life of the nuclide, ρ is rock density (~2.6 g/cm³), E is the pre-burial erosion rate (cm/yr), and Λ is the nucleon attenuation length (160 g/cm²). As the pre-burial erosion rate increases, the pre-burial concentration of the nuclide will decrease. Eq. (1) shows production by only nucleons for simplicity but can be extended to include muon reactions as well (e.g., Granger and Smith, 2000; Balco, 2017). Following burial, the nuclide's concentration will decrease with time:

$$N_{i} = N_{i,inh} e^{-t/\tau_{i}}$$
 (2)

where N_i is the measured concentration of the nuclide. Combining Eqs. (1) and (2) yields a model of nuclide concentration N_i that is a function of pre-burial erosion rate and burial age:

$$N_{i} = \frac{P_{i}}{\tau_{i} + \frac{\rho E}{\Lambda}} e^{-t/\tau_{i}}$$
(3)

Simultaneously solving Eq. (3) for measured concentrations of ²⁶Al and ¹⁰Be yields both the burial age and pre-burial erosion rate, with the assumption that no post-burial production of ²⁶Al or ¹⁰Be has occurred. It is appropriate for dating sediments that have been rapidly buried to depths where production via muons is negligible such as in caves (e.g., Granger et al., 1997), but this assumption is often violated in the case of terrace deposits, which can undergo significant post-burial production of cosmogenic nuclides caused by deeply penetrating muons. Post-burial production raises the measured ²⁶Al/¹⁰Be ratio; as such, burial ages calculated using this approach are minimum deposit ages.

2.1.3. Maximum burial age dating

Post-burial production by muons causes Eq. (3) to underestimate the true age. We can place a maximum bound on the burial age by considering the maximum post-burial production by muons. If we assume that the sampled deposit was previously thicker and has been eroding over time, then the present depth of the sample is its minimum depth since the time of deposition. The production rate by muons at the present depth is therefore the maximum that the sample has experienced, and we can use its current depth to constrain the maximum depositional age. The maximum age may be modeled by adding a post-burial component to Eq. (3):

147
$$N_{i} = \frac{P_{i}}{\tau_{i} + \frac{\rho E}{\Lambda}} e^{-t/\tau_{i}} + P_{i,z} \tau_{i} (1 - e^{-t/\tau_{i}})$$
 (4)

where $P_{i,z}$ is the production rate of a given nuclide at the modern burial depth (at/g/yr). The value of $P_{i,z}$ for a given location may be estimated using exponential approximations (e.g., Granger and Smith, 2000; Schaller et al., 2001; Braucher et al., 2013) or computerized models based on geological calibration sites (e.g., Marrero et al., 2016; Balco, 2017). We calculated muogenic production rates using the parameters: $\alpha = 1$, $\sigma_{0,10} = 0.251~\mu b$, $\sigma_{0,26} = 4.21~\mu b$ (Marrero et al., 2016). As with the minimum burial age approach, Eq. (4) may also be solved simultaneously for measured concentrations of 26 Al and 10 Be. One complication brought on by high post-burial production, however, is that the maximum ages may be unconstrained, placing no upper bound on the true age. We have modified the traditional minimum-maximum burial dating approach to generate relative likelihood functions for the ages of dated deposits, as detailed in Section 4.2.

2.1.4. ²⁶Al/¹⁰Be sample preparation

For this study, quartz sand, quartzite clasts, and chert clasts were collected from terrace deposits at depths ranging from 9-15 m below the contact between the Upland Complex and overlying loess. We sampled four locations for cosmogenic 26 Al/ 10 Be burial dating: the Drum, Kuhn, Mid-South, and Tri-County quarries (Fig. 1). Individual clasts that were large enough for measurement (\geq 4 g) were manually crushed. Smaller gravels were mixed and crushed in the cases of VA-MID (m) and VA-TRI (m). Gravels and sands were sieved to 250-500 μ m and rinsed with deionized water to remove fine materials, then run through a magnetic separator and heavy liquids (lithium heteropolytungstate) to remove contaminant minerals. All samples were subjected to selective dissolution in heated 1% HF/HNO₃. Sample aliquots were subsequently analyzed via inductively coupled plasma optical emission spectrometry (ICP-OES) to determine aluminum content as a test of purity.

Sufficiently pure quartz samples received ~260 µg of ⁹Be carrier and were dissolved in concentrated HF/HNO₃. Aliquots were taken from each dissolved solution to measure final Al content. The samples were then evaporated, and excess Fe/Ti oxides removed via precipitation at pH ~14 in sodium hydroxide. Al and Be hydroxides were precipitated, rinsed, and redissolved prior to separation by cation and anion exchange column chromatography. The isolated Al and Be were converted to aluminum chloride and beryllium nitrate, dried, and decomposed to oxides by calcination with a propane torch. Al and Be oxide powders were then mixed with niobium and loaded into stainless steel cathodes. ²⁷Al/²⁶Al and ¹⁰Be/⁹Be ratios were measured at PRIME Lab via accelerator mass spectrometry (AMS) against the standards of Nishiizumi (2004) and Nishiizumi et al. (2007). Total Al, Be carrier, and AMS measurements are available in the supplementary data section.

2.2.1. (U-Th)/He dating

(U-Th)/He dating of goethite was used to determine the formation age of Fe-oxide cement of the Upland Complex. The goethite cement in the interstitial space of this quartz-dominated sand displays a mostly botryoidal growth texture (see supplementary figures), which is developed on length scales of tens of micrometers. Poly-crystalline goethite aggregates typically retain >90% of radiogenic He at earth-surface conditions and on timescales of millions of years, as shown by previous diffusion experiments and ⁴He/³He studies (e.g., Shuster et al., 2005; Vasconcelos et al., 2013; Hofmann et al., 2017). SEM images reveal homogenous goethitic material without obvious grain boundaries or inclusions of tens to hundreds of micrometers in diameter. Therefore, the goethite cement of the Upland Complex is a valid target phase for (U-Th)/He dating. Previous studies on Fe-oxides formed in weathering environments, most of all duricrusts (e.g. Vasconcelos et al., 2013; Riffel et al., 2016; Allard et al., 2018; Monteiro et al., 2018), have yielded geologically meaningful ages using similar material. Analytical procedures, including laser heating, helium measurement, sample dissolution, and elemental analysis, followed the ones outlined in Hofmann et al. (2020).

These ages provide information on the timescales of post-depositional weathering and soil formation. Fe-rich surficial systems frequently display dissolution of previous generations of Fe-oxide and re-precipitation to form new material (e.g., Hofmann et al., 2017; Monteiro et al., 2018). This cycling of Fe-oxides through dissolution-precipitation reactions leads to an age distribution skewed towards more recent ages. We therefore dated >100 aliquots to explore the temporal range of weathering and the earliest phase of post-depositional weathering, which can yield constraints on the depositional age of the Upland Complex.

2.2.2. Sample preparation

We sampled the Upland Complex for goethite (U-Th)/He dating in four different quarries: De Soto quarry, Drum quarry, Kuhn quarry, and Arlington quarry (Fig. 1). Samples consisted of bulk soil material with Fe-oxide cement and groundwater crusts. Groundwater crusts were crushed to a grain size of ~200-500 μm. Bulk soil material and crushate was sieved to remove material <20 μm and >2 mm, and then density separated using a sodium polytungstate (SPT) solution of density ~3050 kg/m³. The material was mixed with the SPT and centrifuged at 3200 rpm for 30 min. The supernatant was discarded, and the settled material was rinsed several times in distilled water. This process removed most of the quartz and other light minerals and left material highly enriched in Fe-oxides. Samples of the Kuhn quarry were treated with 0.1 M hydroxylamine hydrochloride at room temperature for four hours to selectively dissolve Mnoxide grains (procedure after Chao, 1972).

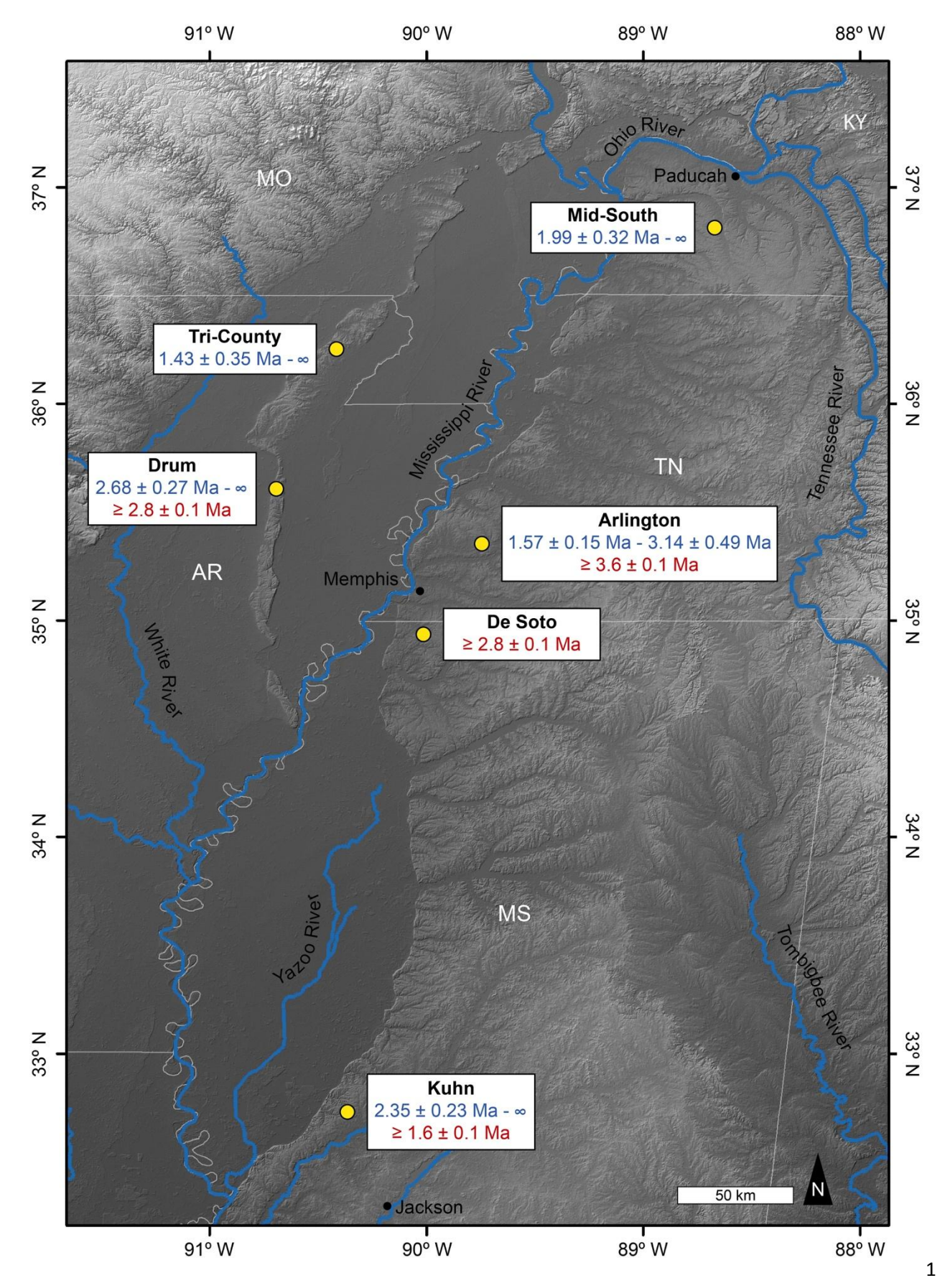


Figure 1. Locations of sites dated with cosmogenic 26 Al/ 10 Be and (U-Th)/He geochronology. Cosmogenic 26 Al/ 10 Be burial ages of terraces are shown above (U-Th)/He ages and represent the 1σ (analytical uncertainty) minimum and maximum ages where available; minimum age constraints derived from the oldest (U-Th)/He ages (with 1σ uncertainty) for each site are shown below burial ages. Note that the Mid-South and Tri-County quarries only have 26 Al/ 10 Be burial ages, whereas the De Soto quarry only has a (U-Th)/He age. ***2-column fitting image***

2.2.3. Analysis

Aliquots of Fe-oxide cement free of visible inclusions and intergrowth with other phases were picked from this material and loaded into Pt tubes. Aliquots representing the center of interstitial goethite cement away from neighboring phases were picked to reduce the effect of possible alpha ejection and implantation. Degassing, ⁴He measurement, dissolution, and ICP-MS measurement of U, Th, Sm, Fe, Mn, Al, and Si followed the goethite protocol described in Hofmann et al. (2020). Procedural He blanks were around 1 pcc (~45 amol) and measured He amounts were at least a factor of three above blank level (>3 pcc). Blanks were interspersed among sets of 6-12 sample measurements. Reported He measurements were blank-corrected using these procedural blank measurements.

Aliquots were screened for being pure Fe-oxide by measuring elemental contributions from substitution for Fe and from other phases. We rejected aliquots based on the following criteria: (1) the Fe-based mass was significantly lower than expected based on the physical dimensions of the aliquot, (2) aliquots with an Al, Si, and Mn content above reasonable limits for goethite stoichiometry, (3) Fe-based mass and trace element concentrations were comparable to other aliquots of the same sample but contained a much higher He concentration and subsequently produced ages that were geologically unreasonable. An elevated He concentration is most likely caused by He implanted from and contained in insoluble mineral inclusions, such

as zircon, and has been observed in previous studies (e.g., Hofmann et al., 2017; Hofmann, 2019).

The mineral phases of samples were identified using Attenuated Total Reflection Fourier-Transform Infrared (ATR-FTIR) spectroscopy by comparing them to known goethite, hematite, and quartz samples. Characteristic peaks for goethite are at 795 cm⁻¹, 899 cm⁻¹, 1662 cm⁻¹, and 1793 cm⁻¹, with an additional broad peak with a center around 3090-3110 cm⁻¹. Quartz peaks are at 1079 cm⁻¹ and 453 cm⁻¹, with an additional doublet at 783 cm⁻¹.

3. Results

3.1.1. Initial ²⁶Al/¹⁰Be geochronology

Van Arsdale et al. (2014) previously dated a remnant of the Upland Complex in Arlington, Tennessee, 15 km northeast of Memphis using cosmogenic 26 Al/ 10 Be in two samples from a Memphis Stone and Gravel Company quarry. These samples were collected at a depth of approximately 10 m below the top of the Upland Complex and processed by G. Balco for AMS measurement. Gravel sample 12-GG-UC2 yielded a minimum burial age of 1.35 ± 0.15 Ma and a maximum burial age of 2.84 ± 0.52 Ma, while sand sample 12-GG-UC1S yielded a minimal burial age of 1.57 ± 0.15 Ma and a maximum burial age of 3.14 ± 0.49 Ma (all 1σ analytical uncertainties). These results indicate that this section of the Upland Complex is at least Early Pleistocene in age and may be Pliocene.

3.1.2. New ²⁶Al/¹⁰Be burial ages

Measured ²⁶Al and ¹⁰Be concentrations are provided in the supplementary data. The minimum ages were generally Pleistocene, with the exceptions of samples VA-DRUM (sand),

MID-1 (quartz gravel), and VA-TRI-52 (chert). Sample MID-1, a single quartz clast, featured an unusually old age and low 26 Al/ 10 Be ratio relative to its counterparts at the Mid-South quarry, indicating that it experienced previous burial. As such, it was excluded from further calculations. Similarly, the chert clast VA-TRI-52 had an excess concentration of 10 Be that lowered its 26 Al/ 10 Be ratio and increased its apparent age. This was attributed to meteoric 10 Be contamination that commonly occurs with cherts and led to the sample's exclusion from the final age estimate. VA-DRUM, being a sand fraction, likely contained minimal reworked material and yielded a valid Pliocene minimum age of 2.68 ± 0.27 Ma (1σ analytical uncertainty).

Pre-burial erosion rates were generally low but can be difficult to quantify when significant post-burial production has occurred. If post-burial production of ²⁶Al/¹⁰Be is unaccounted for, the calculated pre-burial erosion rates will likely overestimate the true values. Conversely, accounting for maximum post-burial production will potentially yield underestimates of pre-burial erosion rates (see Fig. 2). Nonetheless, the pre-burial erosion rates that ignore post-burial production are useful for placing bounds on maximum erosion rates prior to sediment burial (see supplementary table). Sand fractions yielded generally slow pre-burial erosion rates, ranging from 6.6-21.8 m/My. Gravel fractions and individual clasts yielded somewhat higher pre-burial erosion rates, ranging from 7.0-33.9 m/My when the ¹⁰Be-contaminated chert clast was ignored.

Although minimum burial ages for the remaining samples were generally Early Pleistocene and featured low uncertainties, the maximum burial ages were more widely distributed. In most cases, maximum ages were unconstrained toward infinity. These partial maximum burial ages aid in identifying more likely burial ages but leave open the possibility of infinite burial ages. Samples 12-GG-UC2 and 12-GG-UC-1S, both from the Arlington quarry, produced the only completely constrained maximum burial ages. Their respective burial ages permit either a

Pleistocene or Pliocene burial age for the Upland Complex at the Arlington quarry. This wide span of possible ages motivates an additional constraint – (U-Th)/He geochronology – on the true age of the Upland Complex. The high precision of (U-Th)/He dating on goethite cements allows a further constraint on the minimum age of Upland Complex deposits.

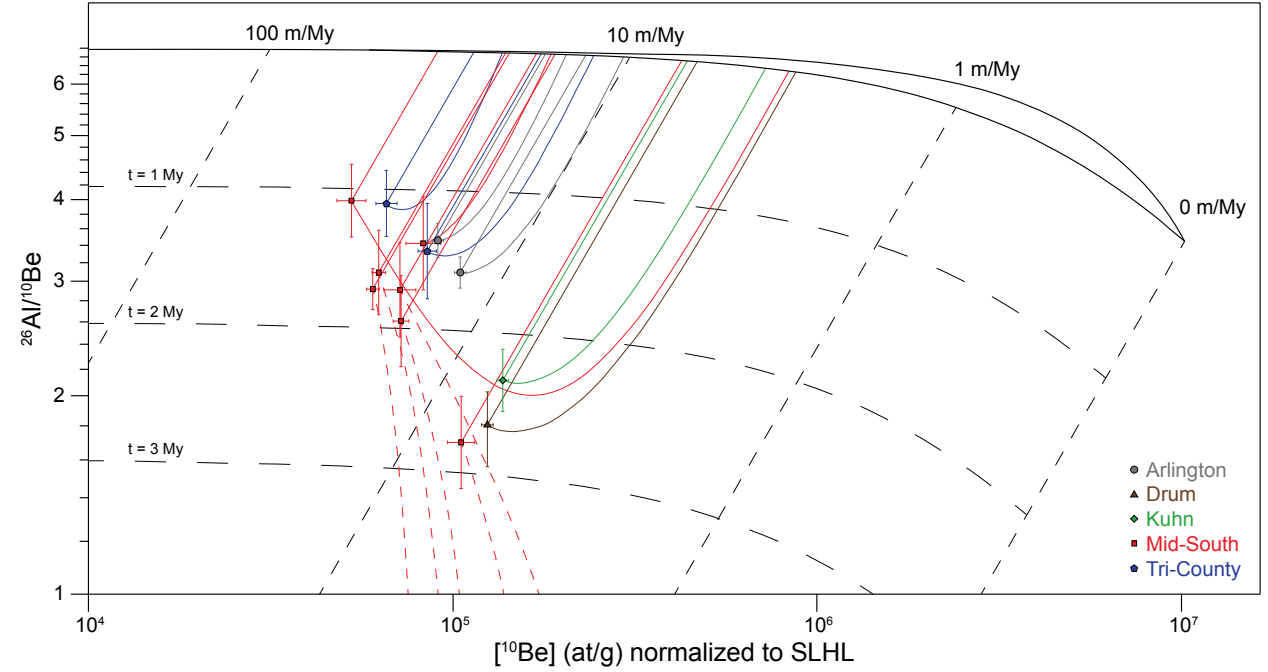


Figure 2. Measured samples and their projected pre-burial histories are shown on the exposure-burial diagram. Simple burial histories that do not account for post-burial production (minimum ages) are represented by straight lines; burial histories that do account for post-burial production (maximum ages) are represented by curves. Samples that yielded indefinite maximum ages have unconstrained burial histories represented by dashed lines. Note that pre-burial erosion rate estimates are lower when post-burial production is incorporated into sample histories. ***2-column fitting image***

3.2.1. (U-Th)/He Results

We acquired (U-Th)/He formation ages of a total of 102 individual aliquots, of which 18 were rejected based on the criteria outlined in the methods section. The ATR-FTIR spectra (Fig.

3) of samples analyzed for (U-Th)/He dating show that they mainly consist of goethite. The spectra also show a minor contribution of quartz in the bulk samples used for ATR-FTIR analysis. The aliquots picked from this material for (U-Th)/He dating were single grains of pure goethite with diameters of several hundred micrometers and did not contain any quartz. Since they are much larger than the mean alpha ejection distance (\sim 20 μ m), no correction for alpha ejection or implantation was applied. A correlation between age and effective uranium concentration (eU), which would indicate detectable loss of U because of sample heating (see Hofmann et al., 2020), was not observed.

(U-Th)/He formation ages of goethite cements from the Upland Complex taken on depth profiles starting just below the "clay gravel" paleosol in the De Soto and Arlington quarries decline with depth (Fig. 4). All (U-Th)/He dates are given with analytical uncertainties to the 1σ level. The oldest ages (2-3.5 Ma) occur close to the contact with the well-developed paleosol. About 0.5 m below the contact, ages range from 0.5 Ma to 2 Ma. Ages are <1 Ma at ~1 m below the contact. A sample of a groundwater crust just above the modern groundwater table (Arlington-D) yielded a near-zero age.

Groundwater crusts from the Drum quarry yielded ages between 0.4 Ma and 3 Ma. A goethite cemented boulder from a depth of approximately 15 m beneath the top of the Upland Complex from the Kuhn quarry yielded ages of 0.1-1.5 Ma, with most ages between 0.2 Ma and 0.4 Ma, and only two aliquots >0.6 Ma.

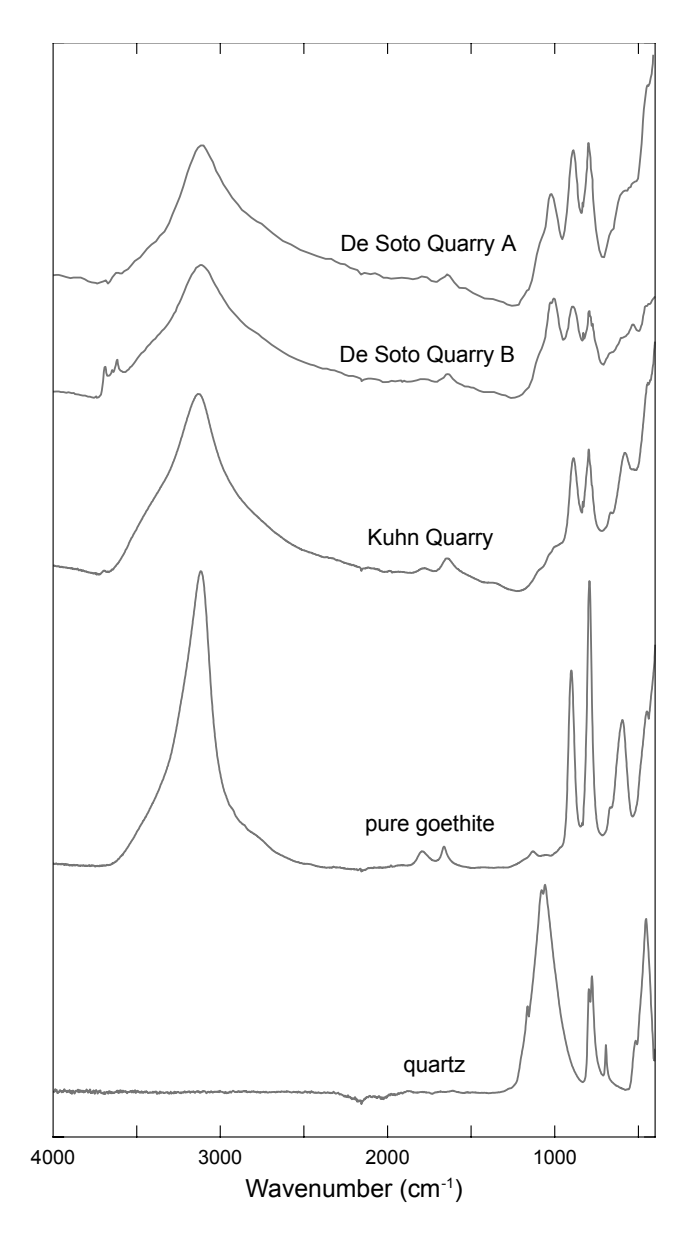


Figure 3. ATR-FTIR spectra of separates from the De Soto and Kuhn quarries compared against pure goethite and quartz. Separates are mostly composed of goethite, with a small amount of quartz present in the bulk material (only goethite was selected for (U-Th)/He dating). Samples from De Soto quarry also show a minor contribution from kaolinite (peaks at 3635 and 3730 cm⁻¹). ***1-column fitting image***

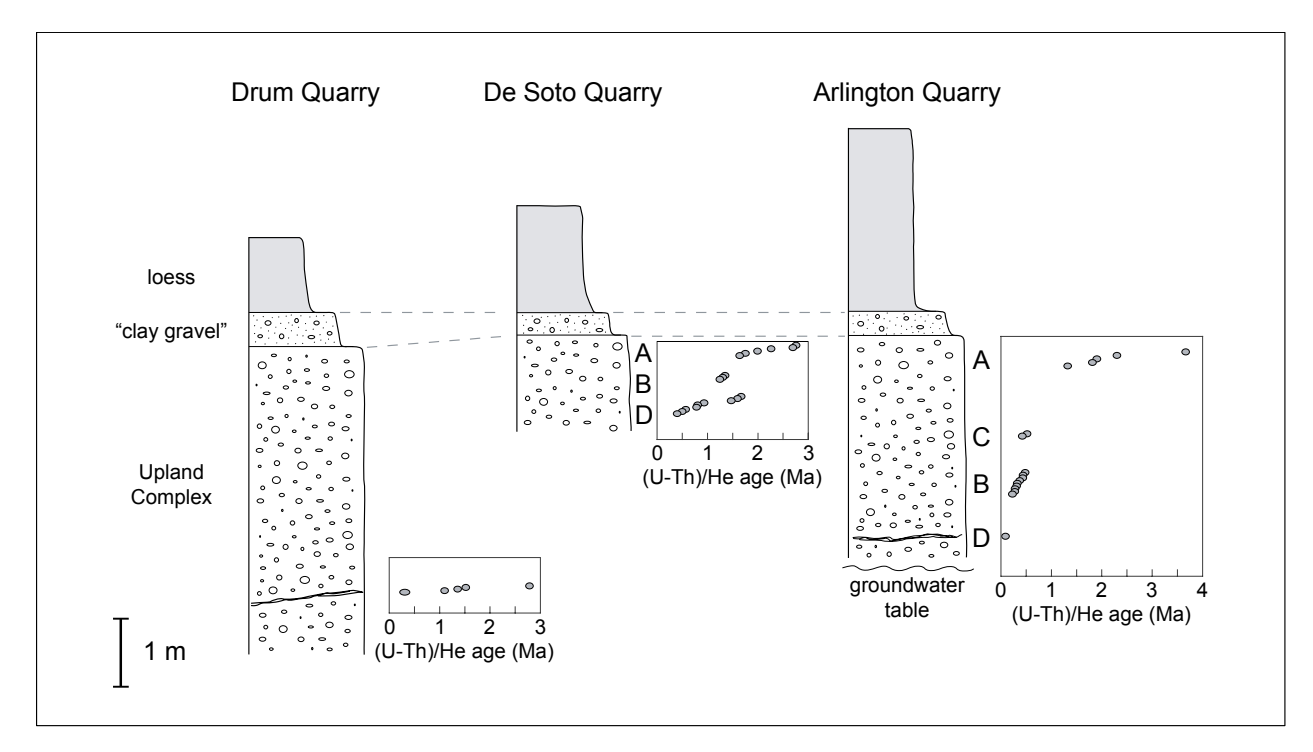


Figure 4. (U-Th)/He dates of goethite cements from the Upland Complex, which is capped by a paleosol ("clay gravel"), and Pleistocene loess. Ages are oldest close to the bottom of the paleosol and decline with depth.

Groundwater crusts (indicated by black streaks in the stratigraphic sections) near the modern groundwater table (Arlington quarry) have a near-zero age. ***2-column fitting image***

336 4. Discussion

4.1. Implications of ²⁶Al/¹⁰Be and (U-Th)/He results

Taken together, the ²⁶Al/¹⁰Be and (U-Th)/He geochronology reveal a Late Neogene history of floodplain and terrace formation followed by post-depositional weathering. Based on ²⁶Al/¹⁰Be ages alone, it appears likely that the Upland Complex formed during the Pliocene or Pleistocene; however, it is not possible to determine whether all dated terraces are the same age. The best ²⁶Al/¹⁰Be constraints on the age of the Upland Complex were sourced from the Arlington quarry, but even these results cannot resolve the Pliocene or Pleistocene age of the Upland Complex. Our estimates of pre-burial erosion rates from sands indicate generally slow

erosion rates that support a pre-glacial origin, but do not conclusively demonstrate a Pliocene age.

345

346

347

348

349

350

351

352

353

354

355

356

357

358

359

360

361

362

363

364

365

The (U-Th)/He ages resulting from this study place basic constraints on the minimum ages of the dated sites, as in-place goethite formation must have postdated the formation of the Upland Complex. The similar distributions of (U-Th)/He ages from the Arlington and Kuhn quarries – mostly Late Pleistocene with rare Early Pleistocene to Pliocene ages – reflect the likelihood that older goethite deposits have likely been dissolved and reprecipitated, skewing the distributions toward younger ages (Fig. 5). An additional indication for this process is that the youngest ages are found close to the modern groundwater table, whereas the oldest ages are found well above the groundwater table. Some young ages may also be the result of intergrowth between older and younger material at length scales below that of an individual aliquot or partial helium-loss in the case of very fine-grained material. This could potentially lead to an underestimation of the minimum age. Though less evident at the DeSoto and Drum quarries, skewed age distributions demonstrate a potential limitation of using goethite formation ages as minimum bounds on the true age of a deposit. Even so, incorporating each site's oldest (U-Th)/He age significantly improved age estimates for three of the four sites dated with (U-Th)/He that featured Pliocene (U-Th)/He ages: De Soto quarry (2.8 \pm 0.1 Ma), Drum quarry (2.8 \pm 0.1 Ma), and Arlington quarry (3.6 \pm 0.1 Ma). Based on (U-Th)/He data alone, it appears that the Upland Complex is a pre-glacial unit as these ages significantly predate the first major Pleistocene glaciation at 2.42 ± 0.14 Ma (Balco and Rovey, 2010).

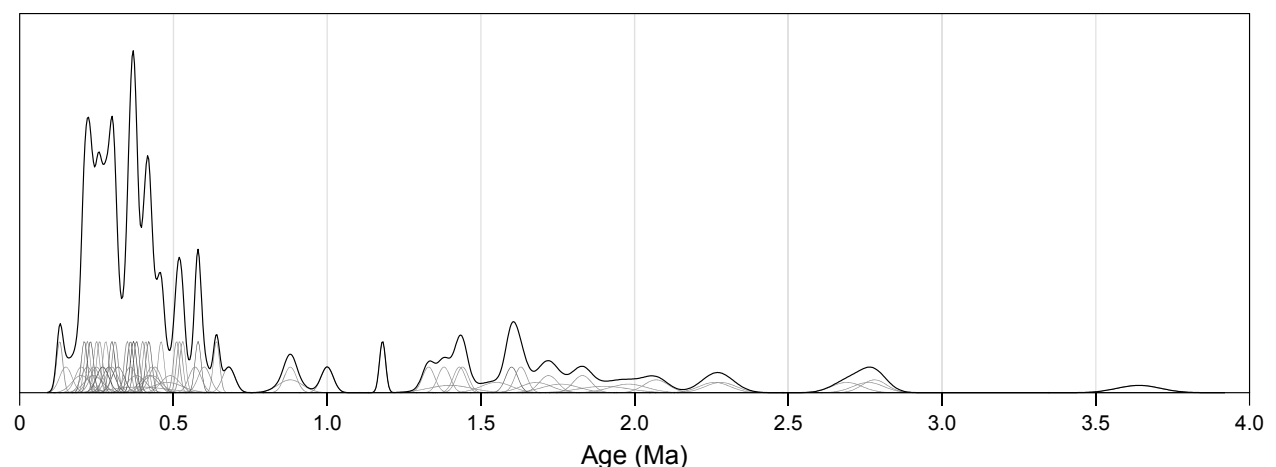


Figure 5. Normal kernel density estimates of (U-Th)/He ages of goethite cements. Individual ages are shown in gray; overall age distribution is shown in black. Note that the age distribution is skewed toward ages <0.5 Ma, reflecting the likely dissolution and reprecipitation of older Fe-oxide deposits. Plot created using camelplot.m MATLAB code by G. Balco, available at http://depts.washington.edu/cosmolab/pubs/gb_pubs/camelplot.m ***2-column fitting image***

4.2. Generating relative likelihood functions for dated deposits

To calculate the permissible range of ²⁶Al/¹⁰Be ages for each sample, we solved Eqs. (3) and (4) for measured concentrations of ²⁶Al and ¹⁰Be. Uncertainties were propagated numerically assuming normal distributions for the isotope measurements. We constructed a likelihood function for the total permissible age distribution of each sample by taking the minimum age from the left (younger) side of the minimum age likelihood function, and the maximum age from the right (older) side of the maximum age likelihood function. For cases with minor post-burial production, this approach yielded closed likelihood functions. In cases where the theoretical post-burial production calculated with Eq. (4) yielded greater concentrations than actually measured, the maximum age likelihood function was unconstrained on the high end.

To generate overall age estimates for individual quarry sites with multiple samples, we

assumed that (1) all sands and gravels of a given terrace deposit were the same age and (2) all (U-Th)/He ages represented minimum ages for the deposit, since goethite formation post-dated terrace deposition. We generated a likelihood function for the oldest (U-Th)/He age at each location that featured constant likelihood for all ages exceeding the (U-Th)/He age. This likelihood function was then multiplied by all of the ²⁶Al/¹⁰Be likelihood functions at that location to generate an overall likelihood function for the site. We opted to multiply, rather than add, likelihood functions to set likelihood to zero in age ranges forbidden by any sample. At locations where only ²⁶Al/¹⁰Be measurements were available (i.e., Mid-South and Tri-County quarries), we multiplied all ²⁶Al/¹⁰Be likelihood functions. This yielded one final likelihood function of permissible ages per quarry, six in total. These likelihood functions were then normalized for each site to generate relative likelihood functions (Fig. 6).

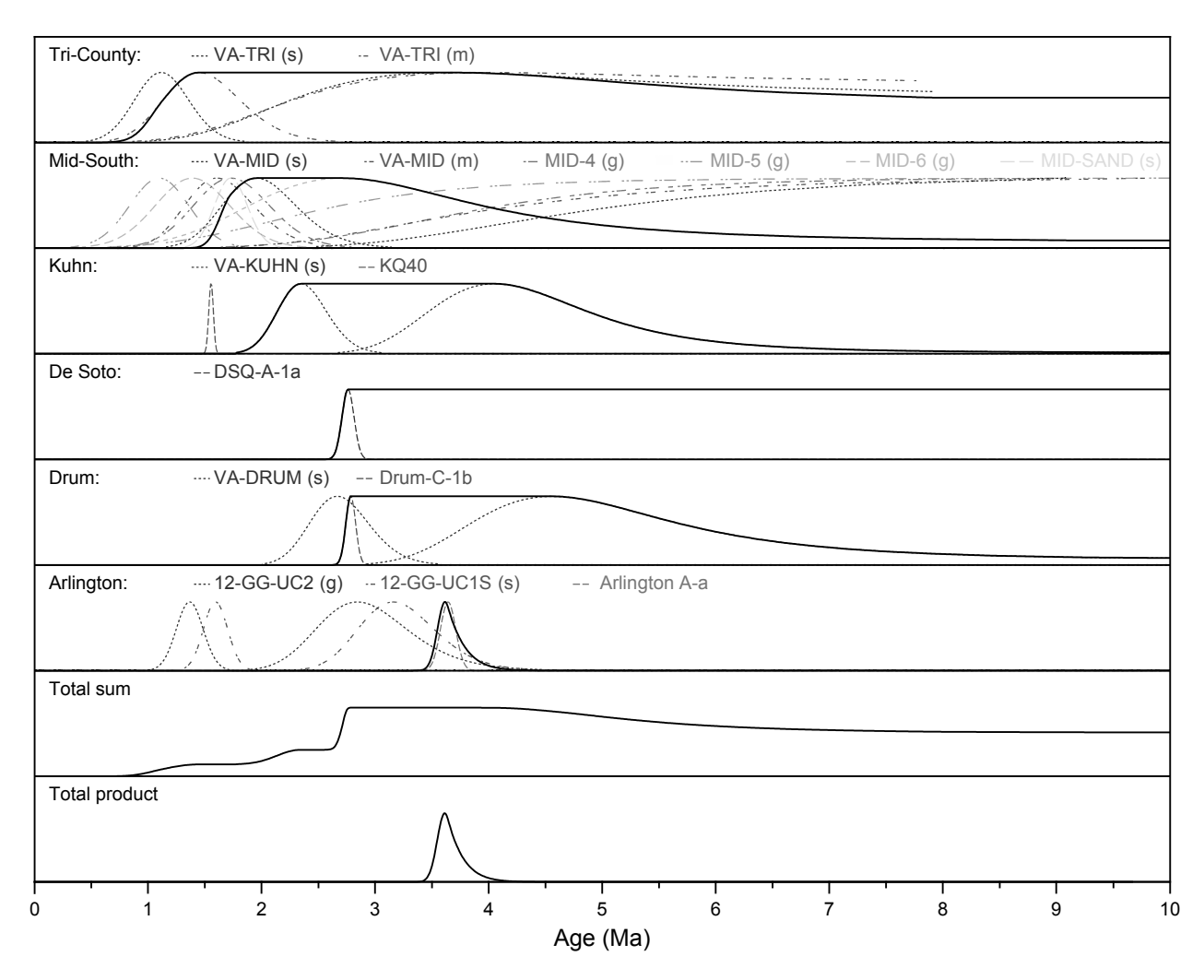


Figure 6. Relative likelihood functions for all sites and the Upland Complex as a whole. Each site's most likely age is represented by a solid line and was calculated by multiplying the normalized likelihood functions for the ²⁶Al/¹⁰Be minimum/maximum ages and the oldest (U-Th)/He age at each site, where available. Dashed lines represent minimum and maximum ages from ²⁶Al/¹⁰Be and (U-Th)/He dating; individual likelihood functions are available in the supplementary figure. The total sum represents the normalized sum of relative likelihood functions from all sites, whereas the total product assumes coeval deposition and was calculated from the normalized product of all relative likelihood functions. ***2-column fitting image***

4.3. Confirming a Pliocene age for the Upland Complex

By combining ²⁶Al/¹⁰Be and (U-Th)/He geochronology, new age estimates emerge for several sites. Kuhn, Mid-South, and Tri-County quarries may still be Pleistocene in age, given

their distributions of ²⁶Al/¹⁰Be and (U-Th)/He ages. It is clear, however, that the deposits at the Arlington, DeSoto, and Drum quarries date to at least the Late Pliocene. Summing all of the likelihood functions yields a curve that sharply increases during the Late Pliocene and reaches a maximum value at 3.61 Ma. Given the high uncertainty of most maximum ages, the relative likelihood function gradually tapers as age increases. If it is assumed that all deposits must be the same age, multiplying the relative likelihood functions for each site yields a well-constrained likelihood function for the age of the Upland Complex. This function is strongly controlled by the likelihood function for the Arlington quarry and also yields a most likely age of 3.61 Ma, with potential ages ranging from 3.40-4.29 Ma (Fig. 6). Whether or not the deposits were coevally formed, these models indicate that the Upland Complex is likely a Pliocene deposit.

The strong dependence of our age estimate on the ages from Arlington quarry is an important consideration when estimating the overall age of the Upland Complex. If the ²⁶Al/¹⁰Be and (U-Th)/He ages from Arlington are discarded when estimating the Upland Complex's age, a slightly different age distribution is revealed. Because of the Pliocene (U-Th)/He ages for goethite deposits at the DeSoto and Drum quarries, it remains likely that the Upland Complex is indeed at least Pliocene in age. The lack of Pliocene goethite at the Kuhn, Mid-South, and Tri-County quarries may reflect dissolution of older generations of cement at those sites and does not preclude a Pliocene minimum age for those locations. Although the uncertainties of ²⁶Al/¹⁰Be maximum ages at the remaining sites remain high, the maximum age distributions for the Drum, Kuhn, and Mid-South quarries all indicate a likely Messinian – but possibly Tortonian – maximum age (Fig. 6). As such, it appears likely that the Upland Complex is at least Pliocene in age and no older than Late Miocene, even in the absence of the measurements at the Arlington quarry.

These age ranges overlap within uncertainty with cosmogenic ²⁶Al/¹⁰Be burial ages for the Grover Gravel deposits in southern Missouri (Rovey et al., 2016) that have been argued to represent the transition from the late Pliocene to the early Pleistocene (Rovey and Spoering, 2020). Our age estimate could correspond to a period of normal or reverse magnetic polarity (Cande and Kent, 1995), so it is not possible to compare with the observation of Rovey and Spoering (2020) that the Grover Gravel was deposited during a period of normal polarity. Our evidence is compatible with the Grover Gravel and Upland Complex being equivalent but does not unequivocally demonstrate this hypothesis.

4.3. The Upland Complex floodplain and Pliocene sea level

Prior to the formation of the Upland Complex, a higher elevation Mississippi River deposited a floodplain mapped as the Citronelle Formation (Dockery and Thompson, 2016), preserved in southern Mississippi. Dockery and Thompson (2016) report that the Citronelle Formation is the remnant of a vast fluvial deposit preserved on drainage divides and is probably Pliocene in age. Near Crystal Springs, Mississippi, the base of the Citronelle is 141 m above msl and slopes south at ~1 m/km. The top of the Upland Complex at the latitude of Crystal Springs is ~115 m amsl, thus illustrating that these do not represent the same level of the ancestral Mississippi River. We hypothesize that incision through the Citronelle Formation and establishment of an Upland Complex floodplain may have been controlled by an Early Pliocene base level drop, perhaps coincident with a currently unidentified continental glaciation.

Our range of possible Pliocene burial ages for different deposits of the Upland Complex may reflect its gradual formation during a prolonged period of base level stability. At the De Soto, Drum, Kuhn, Mid-South, and Tri-County Quarries, we observed overlapping age

distributions during the mid-to-late Pliocene that postdate the Arlington Quarry deposit's formation at ~3.6 Ma. We propose that, given its broad areal extent and thickness, the Upland Complex was gradually deposited during the Pliocene. This gradual mechanism of formation yields similar yet asynchronous age distributions for different dated sites of the Upland Complex, as represented by a broad plateau on the sum of likelihood distributions for all quarries (Fig. 6).

The late Pliocene featured generally high sea levels (Miller et al., 2020) and included the mid Piacenzian Warm Period (mPWP), a well-documented period of elevated temperatures and high sea level (Robinson et al., 2018). Similar conditions were likely responsible for the formation of numerous erosional and aggradational features in North America. Along the east coast of North America, widespread wave-cut shorelines provide evidence of a sea level high stand from ~3.3-2.9 Ma (Rovere et al., 2015). In the Shenandoah Valley, Virginia, 26 Al/ 10 Be dating of alluvial fans and terraces has revealed widespread aggradation at ~3.3 Ma followed by gradual incision (Odom et al., 2019). It appears likely that the Upland Complex also formed as a result of Pliocene aggradation resulting from prolonged base level stability and a high sea level.

5. Conclusion

The age of the Upland Complex has been debated for decades. Previous efforts to date the Upland Complex with cosmogenic ²⁶Al/¹⁰Be improved age constraints but were unable to discern a Pliocene or Pleistocene age. Our combination of ²⁶Al/¹⁰Be burial dating with (U-Th)/He dating of goethite cements demonstrates that the Upland Complex predates the Pleistocene and is very likely Pliocene in age. This supports the hypothesis that the Upland Complex was deposited prior to Pleistocene glaciation.

6. Acknowledgements

We thank Greg Balco for his work to date the Arlington quarry. We wish to thank a number of people who allowed us to sample in their quarries: Jeff Drum (Drum Sand and Gravel, Inc.), Ken McCarley (Kuhn quarry owned by Hammett Gravel Company, Inc.), David Gavin (Mid-South Construction and Old Hickory Clay Company), Dale Gulledge (Tri-County Sand and Gravel quarry). We are also grateful for Ken Miller for providing us with the sea level curve data. Thoughtful suggestions from Atsunori Nakamura, Lewis Owen, and an anonymous reviewer helped us improve the manuscript. This project was partially supported by the National Science Foundation (Grant #1700821) and a PRIME Lab seed grant.

7. Data availability

A complete dataset of (U-Th)/He ages, goethite compositions, and related data are included in the supplementary spreadsheet. This document also includes ²⁶Al/¹⁰Be data, burial ages, and non-blank-corrected AMS data for ²⁶Al/²⁷Al and ¹⁰Be/⁹Be measurements. MATLAB code for likelihood function calculations is included in supplementary documentation.

502	
503	
504	References Cited
505	Allard, T., Gautheron, C., Riffel, S. B., Balan, E., Soares, B. F., Pinna-Jamme, R., et al., 2018.
506	Combined dating of goethites and kaolinites from ferruginous duricrusts. Deciphering the
507	Late Neogene erosion history of Central Amazonia. Chemical Geology 479, 136-150.
808	Anthony, D.M., Granger, D.E., 2006. Five million years of Appalachian landscape evolution
509	preserved in cave sediments. Spec. Pap. Geol. Soc. Am. 404, 39-50.
510	https://doi.org/10.1130/2006.2404(05)
511	Autin, W. J., Burns, S. F., Miller, B. J., Saucier, R. T., Snead, J. I., 1991. Quaternary geology of
512	the Lower Mississippi Valley, in Quat. Nonglac. Geol.: Conterminous US. Geol. Soc.
513	Am., 547-582.
514	Balco, G., 2017. Production rate calculations for cosmic-ray-muon-produced ¹⁰ Be and ²⁶ Al
515	benchmarked against geological calibration data. Quat. Geochronol. 39, 150-173.
516	https://doi.org/10.1016/j.quageo.2017.02.001
517	Balco, G., Rovey, C.W., 2010. Absolute chronology for major Pleistocene advances of the
518	Laurentide Ice Sheet. Geology 38, 795–798. https://doi.org/10.1130/G30946.1
519	Behrman, C., Van Arsdale, R., Kwon, Y., Stockslager, K., Leverett, D., and Lumsden, D., 2019,
520	Drone geologic mapping of an active sand and gravel quarry, DeSoto County,
521	Mississippi. Drones, v. 3, n. 57, p. 1-14. https://doi.org/10.3390/drones3030057
522	Braucher, R., Bourlès, D., Merchel, S., Vidal Romani, J., Fernadez-Mosquera, D., Marti, K.,
523	Léanni, L., Chauvet, F., Arnold, M., Aumaître, G., Keddadouche, K., 2013.
524	Determination of muon attenuation lengths in depth profiles from in situ produced

525	cosmogenic nuclides. Nucl. Instruments Methods Phys. Res. Sect. B Beam Interact. with
526	Mater. Atoms 294, 484–490. https://doi.org/10.1016/j.nimb.2012.05.023
527	Calais, E., Freed, A.M., Van Arsdale, R., and Stein, S., 2010, Triggering of New Madrid
528	seismicity by late-Pleistocene erosion. Nat., v. 466, p. 608-611.
529	https://doi.org/10.1038/nature09258
530	Cande, S.C., Kent, D. V., 1995. Revised calibration of the geomagnetic polarity timescale for the
531	late Cretaceous and Cenozoic. J. Geophys. Res. 100, 6093-6095.
532	https://doi.org/10.1029/94JB03098
533	Chao, T.T., 1972. Selective dissolution of manganese oxides from soils and sediments with
534	acidified hydroxylamine hydrochloride. Soil Sci. Soc. Am. J. 36, 764–768.
535	https://doi.org/10.2136/sssaj1972.03615995003600050024x
536	Chmeleff, J., von Blanckenburg, F., Kossert, K., Jakob, D., 2010. Determination of the ¹⁰ Be half-
537	life by multicollector ICP-MS and liquid scintillation counting. Nucl. Instruments
538	Methods Phys. Res. Sect. B Beam Interact. with Mater. Atoms 268, 192-199.
539	https://doi.org/10.1016/j.nimb.2009.09.012
540	Cooper, F. J., Adams, B. A., Blundy, J. D., Farley, K. A., McKeon, R. E., Ruggiero, A., 2016.
541	Aridity-induced Miocene canyon incision in the Central Andes. Geology 44(8), 675-678.
542	https://doi.org/10.1130/G38254.1
543	Cox, R.T., Lumsden, D.N., Van Arsdale, R.B., 2014. Possible relict meanders of the Pliocene
544	Mississippi River and their implications. J. Geol. 122, 609–622.
545	https://doi.org/10.1086/676974
546	Cupples, W., Van Arsdale, R., 2014. The preglacial "Pliocene" Mississippi River. J. Geol. 122,
547	1–15. https://doi.org/10.1086/674073

548	Dockery, D.T., 1996. Toward a revision of the generalized stratigraphic column of Mississippi.
549	Mississippi Geol. 17, 2–8.
550	Dockery, D.T., Thompson, D.E., 2016. The geology of Mississippi. University Press of Miss.,
551	Jackson, 751.
552	Doering, J. A., 1958. Citronelle Age Problem. Am. Assoc. Pet. Geol. Bull. 42, 764–786.
553	https://doi.org/10.1306/0bda5ac2-16bd-11d7-8645000102c1865d
554	Fisk, H.N., 1944. Geological investigation of the alluvial valley of the lower Mississippi River:
555	Vicksburg, Mississippi. U.S. Army Corps of Eng., Miss. River Comm., 78.
556	Granger, D.E., 2006. A review of burial dating methods using ²⁶ Al and ¹⁰ Be. Spec. Pap. Geol.
557	Soc. Am. 415, 1–16. https://doi.org/10.1130/2006.2415(01)
558	Granger, D.E., Kirchner, J.W., Finkel, R.C., 1997. Quaternary downcutting rate of the New
559	River, Virginia, measured from differential decay of cosmogenic ²⁶ Al and ¹⁰ Be in cave-
560	deposited alluvium. Geology 25, 107-110. https://doi.org/10.1130/0091-
561	7613(1997)025<0107:QDROTN>2.3.CO;2
562	Granger, D.E., Smith, A.L., 2000. Dating buried sediments using radioactive decay and
563	muogenic production of ²⁶ Al and ¹⁰ Be. Nucl. Instruments Methods Phys. Res. Sect. B
564	Beam Interact. with Mater. Atoms 172, 822–826.
565	Guccione, M.J., Prior, W.L., Rutledge, E.M., 1990. The Tertiary and early Quaternary geology
566	of Crowley's Ridge, in Guccione, M., and Rutledge, E., eds., Field Guide to the
567	Mississippi Alluvial Valley Northeast Arkansas and Southeast Missouri: Fayetteville,
568	Arkansas. Friends of the Pleistocene South Central Cell, 23-44.
569	Harrison, R.W., Hoffman, D., Vaughn, J.D., Palmer, J.R., Wiscombe, C.L., McGeehin, J.P.,
570	Stephenson, W.J., Odum, J.K., Williams, R.A., Forman, S.L., 1999. An example of

571	neotectonism in a continental interior - Thebes Gap, Midcontinent, United States.
572	Tectonophysics 305, 399-417. https://doi.org/10.1016/S0040-1951(99)00010-4
573	Hofmann, F., 2019. Iron-oxide geochronology to constrain the formation of soils and paleosols.
574	Calif. Inst. of Technol., PhD thesis.
575	Hofmann, F., Reichenbacher, B., Farley, K.A., 2017. Evidence for >5 Ma paleo-exposure of an
576	Eocene-Miocene paleosol of the Bohnerz Formation, Switzerland. Earth Planet. Sci. Lett.
577	465, 168–175. https://doi.org/10.1016/j.epsl.2017.02.042
578	Hofmann, F., Treffkorn, J., Farley, K.A., 2020. U-loss associated with laser-heating of hematite
579	and goethite in vacuum during (U-Th)/He dating and prevention using high O_2 partial
580	pressure. Chem. Geol. 532, 119350. https://doi.org/10.1016/j.chemgeo.2019.119350
581	Korschinek, G., Bergmaier, A., Faestermann, T., Gerstmann, U.C., Knie, K., Rugel, G., Wallner,
582	A., Dillmann, I., Dollinger, G., von Gostomski, C.L., Kossert, K., Maiti, M., Poutivtsev,
583	M., Remmert, A., 2010. A new value for the half-life of ¹⁰ Be by heavy-ion elastic recoil
584	detection and liquid scintillation counting. Nucl. Instruments Methods Phys. Res. Sect. B
585	Beam Interact. with Mater. Atoms 268, 187–191.
586	https://doi.org/10.1016/j.nimb.2009.09.020
587	Lumsden, D.N., Cox, R.T., Van Arsdale, R.B., Cupples, W.B., 2016. Petrology of Pliocene
588	Mississippi River alluvium: provenance implications 124, 501–517.
589	https://doi.org/10.1086/686997
590	Markewich, H. W., Millard Jr, H. T., Pavich, M. J., Rodbell, D. T., Rich, F. J., Rutledge, E. M.,
591	Ward, L., Van Valkenberg, S., Wysocki, D., 1992. Chronostratigraphic and paleoclimatic
592	data for Quaternary loessial and fluvial deposits in the Mississippi River Valley of
593	Arkansas and Tennessee. Geol. Soc. Am., Abstr. with Progr., A50.

594 Marrero, S.M., Phillips, F.M., Borchers, B., Lifton, N., Aumer, R., Balco, G., 2016. Cosmogenic 595 nuclide systematics and the CRONUScalc program. Quat. Geochronol. 31, 160–187. 596 https://doi.org/10.1016/j.quageo.2015.09.005 597 May, J.H., 1981. The updip limit of Miocene sediments in Mississippi. Geol. Soc. Am. Abstr. 598 with Progr. 13, 1, 29. 599 Miller, K.G., Browning, J. V, Schmelz, W.J., Kopp, R.E., Mountain, G.S., Wright, J.D., 2020. 600 Cenozoic sea-level and cryospheric evolution from deep-sea geochemical and continental 601 margin records. Science Advances 6(20), eaaz1346. 602 Monteiro, H.S., Vasconcelos, P.M.P., Farley, K.A., Lopes, C.A.M., 2018. Age and evolution of 603 diachronous erosion surfaces in the Amazon: Combining (U-Th)/He and cosmogenic 3He 604 records. Geochim. Cosmochim. Acta 229, 162-183. 605 https://doi.org/10.1016/j.gca.2018.02.045 606 Odom, W. E., Granger, D. E., Doctor, D. H., 2019. Dating a mid-Pliocene aggradational episode and subsequent river incision in the Shenandoah Valley with cosmogenic ²⁶Al and ¹⁰Be. 607 608 Geol. Soc. Am., Abstr. with Prog. 51, 5. 609 Olive W. W., 1980. Geologic maps of the Jackson Purchase Region, Kentucky. U.S. Geol. Surv. 610 Misc. Investigations Ser. Map I-1217, scale 1:250,000. Nishiizumi, K., 2004. Preparation of ²⁶Al AMS standards. Nucl. Instruments Methods Phys. Res. 611 612 Sect. B Beam Interact. with Mater. Atoms 223–224, 388–392. 613 https://doi.org/10.1016/j.nimb.2004.04.075

614

615

Absolute calibration of ¹⁰Be AMS standards. Nucl. Instruments Methods Phys. Res. Sect.

Nishiizumi, K., Imamura, M., Caffee, M.W., Southon, J.R., Finkel, R.C., McAninch, J., 2007.

616	B Beam Interact. with Mater. Atoms 258, 403–413.
617	https://doi.org/10.1016/j.nimb.2007.01.297
618	Potter, P. E., 1955a. The petrology and origin of the Lafayette Gravel. Part 1. Mineralogy and
619	petrology. J. of Geology 63, 1–38.
620	Potter, P.E., 1955b. The petrology and origin of the Lafayette Gravel. Part 2. Geomorphic
621	history. J. of Geology 63, 115–132.
622	Riffel, S. B., Vasconcelos, P. M., Carmo, I. O., & Farley, K. A., 2016. Goethite (U-Th)/He
623	geochronology and precipitation mechanisms during weathering of basalts. Chemical
624	Geology 446, 18-32.
625	Robinson, M. M., Dowsett, H. J., Foley, K. M., Riesselman, C. R., 2018. PRISM marine sites—
626	The history of PRISM sea surface temperature estimation. US Geol. Surv., No. 2018-
627	1148.
628	Rovere, A., Hearty, P. J., Austermann, J., Mitrovica, J. X., Gale, J., Moucha, R., Forte, A.,
629	Raymo, M. E., 2015. Mid-Pliocene shorelines of the US Atlantic Coastal Plain — an
630	improved elevation database with comparison to Earth model predictions. Earth-Sci.
631	Rev., 145, 117-131.
632	Rovey, C. W., II, Siemens, M., Balco, G., 2016. Provenance, age, and depositional mechanisms
633	of the Grover Gravel: evidence for multiple erosion cycles, volcanic eruptions, and early
634	glaciations, in Lasemi, Z. and Elrick, S. D. (eds.): 1967-2016 - Celebrating 50 years of
635	Geoscience in the Mid- Continent, 97–124. Guidebook for the 50th Annual Meeting of
636	the Geological Society of America – North- Central Section, April 18–19, 2016. Ill. State
637	Geol. Surv. Guidebook 43.

638 Rovey, C. W., Spoering, G., 2020. Age and provenance of upland gravels in Missouri, USA, and 639 their relationship to Early Pleistocene glaciation. Boreas 49(2), 333-349. 640 Russell, E.E., 1987. Gravel aggregate in Mississippi—Its origin and distribution. Miss. Geology 641 7, 3, 7. 642 Saucier, R.T., 1994. Geomorphology and Quaternary geologic history of the lower Mississippi 643 valley. Vicksburg, Miss., U.S. Army Eng. Waterw. Exp. Stn., 1, 364. 644 Saucier, R. T., Snead, J. I., 1989. Quaternary geology of the Lower Mississippi Valley. Baton 645 Rouge La. Geol. Surv., scale 1:1,000,000, 1 sheet. 646 Schaller, M., von Blanckenburg, F., Hovius, N., Kubik, P. W., 2001. Large-scale erosion rates 647 from in situ-produced cosmogenic nuclides in European river sediments. Earth Planet. 648 Sci. Lett. 188(3-4), 441-458. 649 Shuster, D.L., Vasconcelos, P.M., Heim, J.A., Farley, K.A., 2005. Weathering geochronology by 650 (U-Th)/He dating of goethite. Geochim. Cosmochim. Acta 69, 659–673. 651 https://doi.org/10.1016/j.gca.2004.07.028 652 Van Arsdale, R.B., Arellano, D., Stevens, K.C., Hill, A.A., Lester, J.D., Parks, A.G., Csontos, 653 R.M., Rapino, M.A., Deen, T.S., Woolery, E.W., Harris, J.B., 2012. Geology, 654 Geotechnical Engineering, and Natural Hazards of Memphis, Tennessee, USA. Environ. 655 & Eng. Geosci., v. 18, p. 113-158. https://doi.org/10.2113/gseegeosci.18.2.113 656 Van Arsdale, R. B., Balco, G., Bierman, P. R., Rood, D. H., Rovey, C., Cox, R. T., Lumsden, D. 657 N., Parks, A., 2014. The Pliocene Mississippi River. Geol. Soc. Am., Abstr. with Prog. 658 46, 228. 659 Van Arsdale, R.B., Bresnahan, R., McCallister, N., Waldren, B., 2007. Upland complex of the

central Mississippi River valley: Its origin, denudation, and possible role in reactivation

661	of the New Madrid seismic zone. Spec. Pap. Geol. Soc. Am. 425, 177-192.
662	https://doi.org/10.1130/2007.2425(13)
663	Van Arsdale, R., Cupples, W., 2013. Late Pliocene and Quaternary deformation of the Reelfoot
664	rift. Geosphere 9, 1819–1831. https://doi.org/10.1130/GES00906.1
665	Van Arsdale, R.B., Cox, R.T., Lumsden, D.N., 2019. Quaternary uplift in the lower Mississippi
666	River valley. J. Geol. 127, 1–13. https://doi.org/10.1086/700405
667	Vasconcelos, P. M., Heim, J. A., Farley, K. A., Monteiro, H., & Waltenberg, K., 2013. 40Ar/39Ar
668	and (U-Th)/He-4He/3He geochronology of landscape evolution and channel iron deposit
669	genesis at Lynn Peak, Western Australia. Geochimica et Cosmochimica Acta 117, 283-
670	312.
671	Willman, H.B., Frye, J.C., 1970. Pleistocene stratigraphy of Illinois. Ill. State Geol. Surv. Bull.
672	94, 204.